Evaluating Power and Environmental Performance in Mobile Microgrid Generator Systems

C. Lute[a], J. Cale[a,*], G. Ross[a], J. Tillotson[a], D. Moorman[b], M. Dorflinger[c]

[a]*Colorado State University, 200 W. Lake St., Fort Collins, CO, USA*
[b]*Moser Energy Systems, 260 Craig Thomas Blvd., Evansville, WY, USA*
[c]*LexTM3 Systems, 15751 SW. 41st St. #300, Davie, FL, USA*

Abstract

Mobile microgrid generator systems can provide power to electrical loads during grid outages and for off-grid applications. These systems are often configured using conventional generator sets, but can also be used with parallel energy storage. The addition of energy storage may provide advantages in terms of power quality and emissions. This paper introduces a procedure to experimentally assess mobile microgrid generator systems operating on natural gas (NG) fuel in conventional and energy storage coupled types, for several power and environmental emissions metrics: thermal efficiency, voltage and frequency stability, harmonic distortion, and air pollution from total hydrocarbons (THC), carbon monoxide (CO), nitrogen oxides (NO_x), and carbon dioxide (CO_2). The analysis of thermal efficiency and detailed gas composition and engine emissions analyses are described. Also included is a method of synthesizing realistic load profiles for laboratory testing, based on statistical sampling of metered load data. Implementation of the proposed test procedure is experimentally demonstrated on two types of mobile microgrid generator systems of differing engine sizes: a conventional 22 L NG generator set and a hybrid system consisting of an 11 L NG generator set, in parallel with battery energy storage. Significant differences in power quality, fuel usage and emissions metrics were observed between the two systems using the procedure. Measurements using the procedure are also used as inputs to an example economic and environmental cost analysis for a remote microgrid design. These findings suggest the potential usefulness of the procedure for evaluation of competing generator sizes and configurations, which can also provide input to mobile microgrid designs.

Keywords: microgrid, mobile, hybrid, power quality, emissions

1. Introduction

MICROGRIDS are a solution for maintaining power delivery to electrical loads during grid outages or other contingencies; their effectiveness in this regard has been demonstrated in many use-cases in recent decades [1]. Two broad classifications of microgrid types are facility-based and remote ("off-grid") configurations [2, 3]. In facility-based microgrids, some or all of the electricity is nominally obtained from a local electrical power system (EPS); during loss of power, microgrid generation assets are used to supply

*Corresponding author
Email addresses: Chris.Lute@colostate.edu (C. Lute), James.Cale@colostate.edu (J. Cale), Garrett.Ross@colostate.edu (G. Ross), James.Tillotson@colostate.edu (J. Tillotson), darrin@moseres.com (D. Moorman), mdorflinger@lextm3.com (M. Dorflinger)

the deficit. In facility-based microgrids, generation is often installed in predesignated building(s) serving 'critical' facility loads [4]. In this configuration, microgrids essentially serve as a replacement to traditional energy management plans for critical facilities, which historically relied on backup generators.

In contrast, in remote microgrids there is generally not a local EPS available to provide power; electricity is nominally obtained by the microgrid assets alone. The primary source of power in remote applications is commonly provided by a prime mover (e.g., diesel or natural gas engine, wind-turbine) coupled to an electrical motor/generator, referred to collectively herein as 'genset.' Generator systems for remote microgrids are often mobile (i.e., trailer-mounted) to allow transportation to remote and/or off-grid locations.

A shortcoming of facility-based microgrids is that fixed generator locations—determined *prior* to a grid contingency event—may prove non-optimal during an actual disaster. This is because emergency events (e.g., fire, flood, pandemic) often evolve spatiotemporally [5]. Under these conditions, the movement of humans or resources over time influences the optimal choice of mobile generator location(s). For this reason, recent research has explored the potential advantages of employing mobile generators to provide power to *facility* loads, wherein mobile microgrid systems are moved and connected to optimal building or grid locations; these locations are allowed to change dynamically as the event unfolds [6].

The ability to provide microgrid configurations in an EPS using mobile microgrid generator sets is constrained by the frequency deviation expected during critical load restoration (CLR). In [6], these frequency deviations were estimated using a basic diesel generator model with benchmark parameters. However, the combination of energy storage with traditional generator sets can significantly reduce frequency deviations [7], and thus potentially enable a larger set of possible—and potentially Pareto optimal—microgrid configurations beyond that considered in [6]. In addition, many critical facility loads (e.g., military bases, hospitals, data centers) are in locations with available natural gas lines, obviating the need for diesel storage tanks and frequent refueling. On the other hand, natural gas (NG) engines provide lower load acceptance compared to diesel generators [8]. Mobile generators composed of a combination (herein "hybrid") of a NG generator set with battery energy storage may provide the best overall alternative; a method to experimentally compare hybrid versus traditional generator systems in microgrid use-cases is therefore desirable. Finally, semi-permanent or even temporary installation of generator sets may require emissions permitting. Since permitting fees are based on engine power rating [9], experimental comparison and analysis of trade-offs between engine size, fuel sources and emissions, and the cost of combined energy storage are also needed.

Differences in the performance of conventional versus hybrid generator systems in terms of power quality, environmental and economic value, and specific impacts from the use of NG as a primary fuel source have been described in the literature. In [8], the authors describe the characteristics of the transient response of NG in comparison to diesel engines and cite potential advantages of NG engines in terms of lower emissions, higher efficiency, reduced carbon footprint and the potential use of alternative fuels. They also indicate that load management strategies could further mitigate transients and enable higher efficiency in NG engine types. In [7], the researchers described a robust control strategy for use in mobile microgrid diesel generators, showing a reduction in frequency deviation in hybrid versus conventional generators. However, the studies in [7, 8] were based on modeled performance; they did not include experimental steps or measurements of actual power quality or dynamic performance in NG or diesel engines.

Some research has been conducted analyzing the potential environmental advantages of hybrid generator systems. In [10] the authors analyze conventional heavy fuel oil generators in combination with battery energy storage for powering medium-sized ocean vessels. In their research, carbon dioxide (CO_2) emissions were compared between the hybrid and conventional power systems under two case studies, where it was found in simulation that an 8.6% –20.7% reduction in CO_2 emissions could be achieved, depending on electrical load conditions. This study includes modeled gas emissions in the scenarios; however, the work

in [10] again relied on modeled engine performance using computer simulation rather than experimental measurements to quantify emissions under representative test conditions.

Prior literature has investigated economic differences between hybrid and conventional generator systems. In [11], the authors analyzed the comparative economics of NG versus diesel as the fuel source for backup generators. Their analysis included additional revenue streams from grid services, and some case studies included additional generation assets such as solar photovoltaics (PV) and battery energy storage. The authors found in their case studies that NG generator types had lower fuel costs per kilowatt-hour of energy generation compared to diesel. However, lower capital costs of diesel generators could result in higher economic value over NG generators on a net present value (NPV) basis. The research in [12] described a comparative analysis and optimal sizing a of system comprising solar PV, wind, battery and biodiesel generator where the biodiesel fuel served as a replacement to petroleum diesel. The study and optimization considered the emissions output and total economic value of the system. As in the previous studies, [11, 12] were based on modeled performance, and did not include experimental measurements as inputs. The analysis in [11] assumed fixed backup building generators that could provide grid-services, as opposed to mobile systems; the PV and energy storage system power were also analyzed independently of the generators. Furthermore, neither of the studies in [11, 12] considered the use of parallel energy storage to reduce the generator engine size to reduce fuel, emissions, or permitting costs in mobile or temporarily-installed systems which is used in the economic and environmental cost assessment performed in this paper.

In contrast to previous literature, this paper introduces a procedure to experimentally measure several power quality and environmental performance metrics in mobile microgrid generators, to provide empirical inputs to microgrid design studies. In particular, a procedure is described and demonstrated to assess and compare conventional versus hybrid NG generator systems in terms of: (*i*) thermal efficiency under constant and stochastic loads, (*ii*) voltage and frequency deviations under load step changes, (*iii*) steady-state voltage and current distortion under constant loads, and (*iv*) emissions pollutants from total hydrocarbons (THC), carbon monoxide (CO), nitrogen oxides (NO_x), and carbon dioxide (CO_2). Using measurements obtained from the procedure, a comparison of economic and environmental costs in conventional versus hybrid NG generators for an example off-grid microgrid design study is also presented.

Key contributions of this paper include:

- A procedure for experimental evaluation and comparison of conventional and hybrid NG mobile microgrid generator systems, in terms of several power and environmental metrics;
- A description for calculating thermal efficiency, performing detailed fuel composition and gas emissions analyses;
- A method for synthesizing realistic load profiles for laboratory testing using statistical sampling;
- Demonstration of the above experimental and analytical steps of the procedure on conventional and hybrid NG generator system hardware at 0–350 kW power levels;
- Illustration of an economic and environmental costs comparison between conventional and hybrid generator alternatives in an example off-grid microgrid design using the experimental measurements.

The remainder of this paper is structured as follows. Section 2 provides general background on conventional and hybrid generator systems. An outline of the proposed test procedure is given in section 3. Section 4 describes the load synthesis step of the procedure. In section 5 the microgrid testbed and devices under test for the experimental work are described. Experimental measurements of thermal efficiency, power quality, and emissions are described, analyzed and discussed in sections 6-8, respectively. Section 9 presents an example economic and environmental cost evaluation using measurements obtained from the procedure. Concluding remarks are provided in section 10.

Notation: In the following sections, bold faced letters are used to denote matrices or vectors; non-bold letters are used for scalar quantities; $\{\cdot\}^T$ represents the matrix transpose operator; $|\cdot|$ symbolizes the absolute value of a real number or cardinality of a set; $||\cdot||$ denotes the magnitude of a complex number; $g(x;\alpha)$ symbolizes the evaluation of function g with variable input x and fixed parameter(s) α; the compact notation

$$\mathbf{f}^x_{abc} := \begin{bmatrix} f^x_a & f^x_b & f^x_c \end{bmatrix}^T, \tag{1}$$

where f can represent voltage or current, subscript a (b or c) represents electrical phase a (b or c), and superscript x is a descriptive label.

2. Background on Conventional and Hybrid Generator Systems

Mobile generator systems commonly employ reciprocating engines, shaft-coupled to a synchronous generator (SG), along with control circuitry for regulating the frequency and voltage of the generator output. A simplified conventional generator system is depicted in Fig. 1.

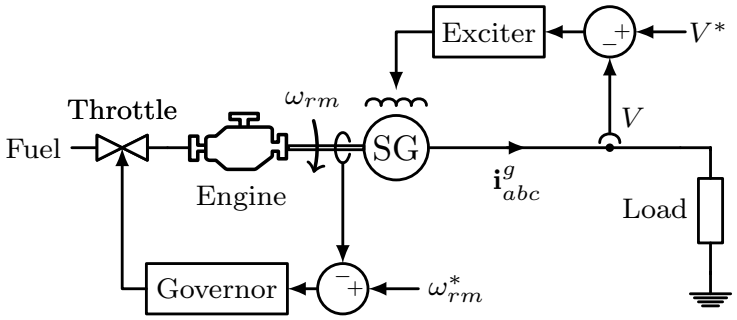

Figure 1: Simplified depiction of a conventional generator system.

As shown in Fig. 1, the engine is supplied by a fuel source (e.g., diesel, NG) and fuel flow is regulated by a throttle valve. Internal combustion within the engine drives a set of reciprocating pistons. Linear piston action is translated into rotational motion of the engine shaft, which rotates at angular velocity ω_{rm}. The engine shaft is coupled to the rotor shaft of the SG. The SG provides electrical currents $\mathbf{i}^g_{abc}$ to the load (note that the electrical portion of the diagram in the bottom-right side of Fig. 1 is drawn in 'one-line' format.) In synchronous generators, the angular electrical frequency $\omega_e = \omega_r$ where $\omega_r = (P/2)\omega_{rm}$ is referred to as the 'electrical angular velocity' of the rotor and P is the number of magnetic poles in the motor [13]. The line electrical frequency is thus indirectly controlled by the governor, which regulates fuel flow to the engine via the throttle valve to achieve the commanded mechanical speed ω^*_{rm} necessary to produce phase voltages at the desired electrical line frequency. Measured line (rms) voltage of the SG is denoted V in Fig. 1; this voltage measurement is compared to the desired voltage V^* in the exciter, which adjusts the excitation voltage of the field winding to achieve the desired generator output voltage.

In conventional generator systems, there are trade-offs when selecting the engine type and fuel source. Diesel engines are commonly used because of their superior cold load-pickup capabilities; diesel engines respond to black-starting and large load steps with relatively small frequency deviations. In contrast, NG is less dense than diesel fuel and consequently, NG engines require an extra compression stage (not shown in Fig. 1) which slows the governor response [8]. However, diesel generators require frequent refueling, which can be problematic in the event of prolonged operation. In these instances, if an NG supply is

available (e.g., pipeline, well-head) NG would be a more reliable and lower cost fuel supply over diesel [11]. Beyond the higher reliability and lower fuel cost, NG is nominally a cleaner burning fuel with reduced emissions compared to diesel [14].

On the other hand, in addition to the slower frequency response in NG engines compared to diesel engines, NG engines can produce noxious 'combustion slip' under low load conditions [14]. Combustion slip refers to unburned fuel passing through the exhaust stream. While diesel engines can also exhibit incomplete combustion under low loads (resulting in 'wet-stacking'), in NG engines combustion slip is predominantly composed of methane [15]. Methane is a greenhouse gas, so excessive combustion slip can negate the positive climate impact of NG fuel over diesel [16].

In light of the above trade-offs between diesel and NG engines, it may be desirable to use NG generator sets where possible to take advantage of inexpensive and (nominally) cleaner-burning fuel, if they can also provide load-pickup at least comparable to diesel engines. A solution to achieve this objective, while also minimizing combustion slip and associated methane emission, is to combine the NG generator set with a parallel battery energy storage system. This "hybrid" configuration with a conventional genset in parallel with battery energy storage employs a design well-established in hybrid electric vehicles [17]. A simplified depiction of a mobile hybrid generator system using this configuration is shown in Fig. 2.

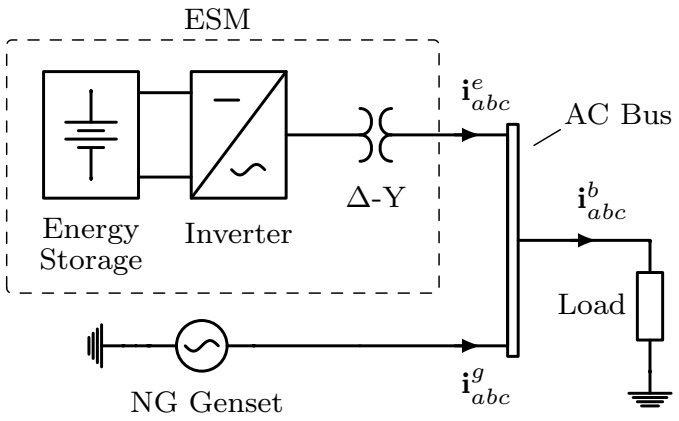

Figure 2: Simplified depiction of an NG mobile hybrid microgrid genset.

In Fig. 2, the battery energy storage system, DC to AC inverter, and output transformer comprise the energy storage module (ESM). The output of the ESM is connected in parallel with a conventional genset (depicted in Fig. 1) through a common AC bus. The ESM and genset provide electrical currents $\mathbf{i}^e_{abc}$ and $\mathbf{i}^g_{abc}$, respectively. Total bus current $\mathbf{i}^b_{abc} = \mathbf{i}^e_{abc} + \mathbf{i}^g_{abc}$ supplies the load.

During start-up and load changes, power-electronic switching and controls in the ESM can provide nearly instantaneous current injection to assist the engine response, allowing even NG-based hybrid generator systems to maintain stiff frequency and voltage regulation (see section 7). During low load scenarios, excess generation capacity can be used to charge the ESM, keeping the engine close to rated load, thereby reducing combustion slip. Under very low load conditions, the conventional generator can be switched off entirely, allowing the microgrid load to be powered from the ESM alone.

For clarity and preciseness, in the remainder of this paper: "genset" refers collectively to any engine and coupled SG; "hybrid generator system" consists of a genset and an ESM, connected to a common AC bus; a "conventional generator system" is synonymous with "conventional genset" and distinguished from a hybrid generator system by a lack of ESM; "generator system" refers collectively to either a conventional or hybrid generator system.

3. Test Procedure

The steps used in the proposed procedure to compare conventional versus hybrid generator systems are as follows:

1. *Synthesize Representative Load Data*. In this step, field measurements of load under actual operating conditions (which the generator systems will supply) are probabilistically sampled to create randomized load sequences for laboratory emulation in step 5). This process is described more fully in section 4.
2. *Build Microgrid Experimental Testbed*. This step includes all electrical wiring and gas pipeline connections to enable the microgrid experiment to be electrically isolated from utility power. Also included is the automation of load bank step changes and the installation of all data acquisition for electrical and gas emissions measurements. Testbed details are given in section 5.
3. *Install Sample Generator Set in Microgrid Testbed*. For each generator system under test, provide electrical and gas pipeline connection (as needed) and setup data acquisition; see more details in section 5.1.
4. *Perform Steady-state Test Sequence*. In this test sequence, the generator system is run at various load levels which represent a percentage of rated power. The generator system is allowed to reach steady-state before measurements are taken. This step includes:
   4.1) Measurements for thermal efficiency
   4.2) Emissions measurements
   See sections 6.2 and 8.2.
5. *Perform Stochastic Load Test Sequence*. In this test sequence, the generator system is run at randomized loads to emulate actual operating conditions. This step includes:
   5.1) Measurements for thermal efficiency
   5.2) Emissions measurements
   See sections 6.3 and 8.3.
6. *Perform Step-Changing Load Test Sequence*. In this test sequence, the controllable load bank is controlled to provide load step-changes. Transient and steady-state response of the generator system are measured, to include:
   6.1) Transient voltage deviation measurement
   6.2) Transient frequency deviation measurement
   6.3) Steady-state total harmonic distortion measurement
   See sections 7.
7. *For each generator set under test, go to step 4).*
8. *Analyze Test Results*. In this final step, measurements taken during the previous test sequences are used to quantify and compare the generator systems in terms of power quality and emissions metrics. Governing formulae and the analysis process is described sections 6-8.

4. Load Synthesis

This section describes a method for synthesizing a load profile that represents—in a probabilistic sense—realistic operating conditions for generator system experimentation required in step 5) of the test procedure.

First, time-varying measurements of load under field operating conditions are obtained. These measurements are then binned into groups of power ranges and ordered by power level, to form an empirical histogram. From the histogram, a cumulative distribution function $F_X(x)$ is obtained, where $X \in \mathbb{R}_+$ is a random variable denoting power level; $x \in \Omega$ is a specific observation of the random variable X; $\Omega = (0, P_{max})$ is the sample space, where P_{max} is the maximum (load) power in the set Ω.

From the cumulative distribution, a set of samples $\mathcal{S}$ is obtained using inverse transform sampling [19] in the following manner. Let $U(0,1)$ denote a uniform distribution over the range $(0,1)$, and $u \sim U(0,1)$ a sample from the distribution. Then, for $k = 1, \ldots, |\mathcal{S}|$, sample $s_k \in \mathcal{S}$ is assigned by the following procedure:

1. Draw a sample $u_k \sim U(0,1)$.
2. Set s_k to the value x such that

$$F_X^{-1}(u_k) := \inf\{x \mid F_X(x) \geq u_k\}, \tag{2}$$

where $\inf\{\cdot\}$ is the infinum function, used in (2) because the empirical distribution function is generally not invertible.

For concreteness, the procedure above is now applied to measurements of load data from a remote microgrid generator system application: a land-based drilling platform, which is emulated in the experiments described in ensuing sections. Fig. 3 shows the time-varying load profile over $2,000$ hrs, with sampling interval of 1 hr. The cumulative distribution for the load measurements is shown in Fig. 4.

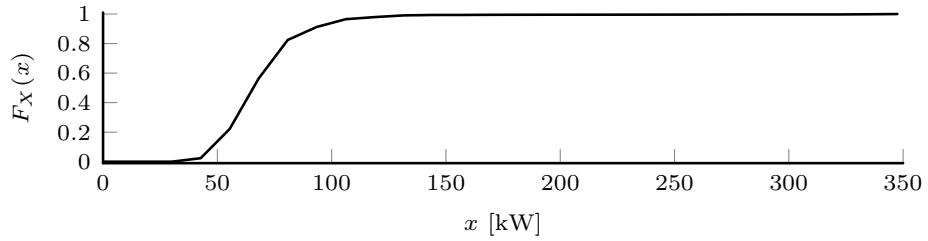

Figure 3: Field measurements of load, remote drilling application.

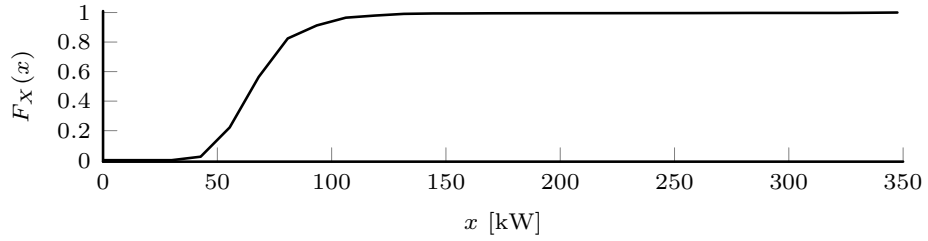

Figure 4: Cumulative distribution function for load measurements in Fig. 3.

As shown in Fig. 3, the load profile consists of a relatively constant 'base load' for long durations (e.g., for on-site lighting), interspersed with large but infrequent power demands; this load characteristic is common in drilling and excavation processes.

A set of 60 samples from the cumulative distribution is shown in Fig. 5; as shown in the figure, the samples are mostly drawn from the base load region (between 50–100 kW), while loads over 300 kW are relatively infrequent, as expected.

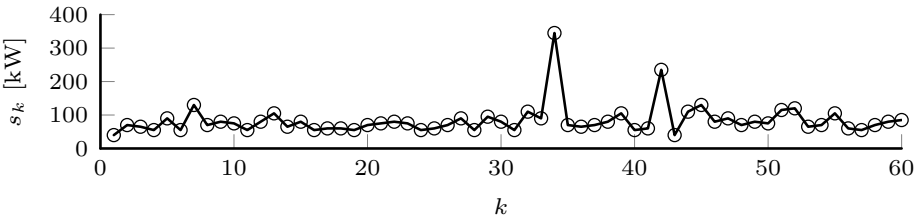

Figure 5: Simulated samples of load measurements in Fig. 3.

5. Microgrid Experiment

This section describes the microgrid experimental testbed used to obtain power and emissions measurements on generator systems and details on the specific systems under test. The testbed and all experiments described in this section were conducted at the Powerhouse Energy Campus ("Powerhouse") at Colorado State University (CSU).

5.1. Description of Microgrid Testbed

The microgrid testbed comprised: power distribution cabling and equipment, NG fuel line and flow meter, emissions measurement system, controllable resistive-inductive ("RL") load bank, load bank control console, and high-speed data acquisition system (DAQS). A depiction of the testbed (with NG-hybrid generator system under test) is shown in Fig. 6.

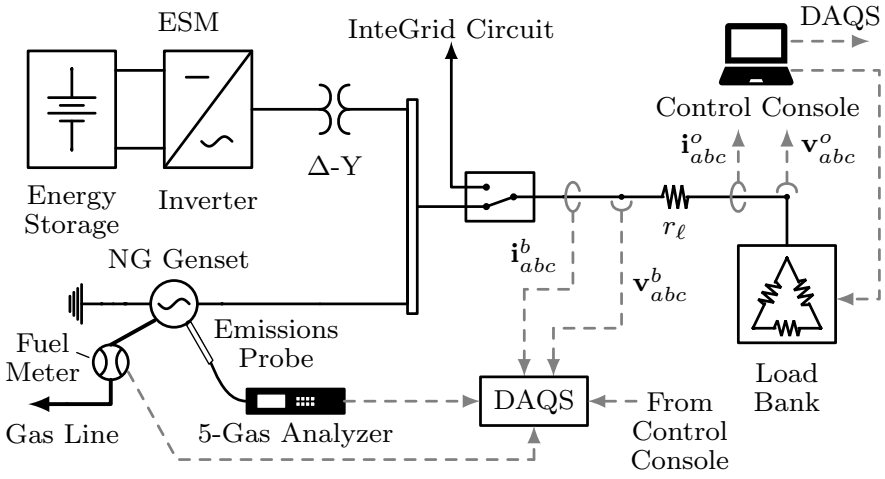

Figure 6: Microgrid experimental testbed, NG-hybrid generator system under test.

As shown in Fig. 6, generator systems were connected to the load through a 800 A transfer switch located in switchgear inside the Powerhouse; the other pole of the transfer switch was connected to the Spirae InteGrid Test and Development Laboratory (not used in this work) [20]. The state of the transfer switch and load bank settings were monitored and configured using a Scheider Electric ClearSCADA interface ("Control Console" in Fig. 6), communicating via Modbus/TCP.

High-speed measurements of bus current and voltage on the load side of the transfer switch upstream from the load, $\mathbf{i}^b_{abc}$ and $\mathbf{v}^b_{abc}$ respectively, were obtained by the DAQS using a Bitronics M571 power meter. Voltage measurements were made directly; current measurements were obtained via Flexcore 800:5A current transducers (CTs). Voltage measurements had a rated accuracy of 0.1% while the Flexcore CTs had a rated 0.3% accuracy. High-speed waveform capture was also performed at this same measurement location, using an AEMC 300-10-2-10-HF current probe rated for 1 MHz, connected to phase C. This current probe

was connected to a Keysight MSOX3012T 100 MHz mixed signal oscilloscope. High-speed voltage capture was obtained using a Keysight N2791A high voltage differential probe, connected across phases A and C.

A 400 kVA RL load bank, manufactured by LoadTec, provided a Δ-connected resistive (only) load to the generator systems during testing. The ClearSCADA control console measured low frequency current and voltage updates directly at the load, $\mathbf{i}^o_{abc}$ and $\mathbf{v}^o_{abc}$ respectively, and allowed the creation of both static and time-varying load profiles. Load profile setpoints were sent to the load bank from the control console via Modbus commands; real power commands had a maximum update rate of 1 S/s with 5 kW resolution, summed across all phases. Cable resistance, r_ℓ, between the high-speed measurement points and load bank terminals was measured as 9.23 mΩ per phase, at conductor temperature 75°C.

The mobile, trailer-mounted generator systems were physically located outside of the Powerhouse during testing. Size 350 MCM copper flexible welding cables exited the building and connected to the AC bus terminals of the generator systems. Inside the building, these cables transitioned to a set of three 4/0 AWG aluminum XHHW conductors per phase. These were spliced into an existing set of three 4/0 copper flexible welding cable conductors per phase, connected to the transfer switch.

To provide NG fuel to the generator systems, an existing 3/4" (19 mm) NG fuel line in the Powerhouse was tapped and routed to the test engine locations. The line mated with a 2" (51 mm) female NPT fitting on the gas engine. Fuel used in testing was pipeline NG; based on a set of four sample measurements taken over three months just prior testing, the gas mixture was found to consist of 85–90% methane, 8–9% ethane, and the remainder consisting of a mix of higher hydrocarbons, nitrogen, and carbon dioxide. A Fox Thermal model FT2A inline fuel meter was used to measure the instantaneous mass flow rate of the fuel going into the engine in standard cubic feet per minute (SCFM) and converted to cubic meters per second[1]. The FT2A fuel meter produced a 4–20 mA output for flow rates of 0–80 SCFM (0–3.78$\times 10^{-2}$ m^3/s). A 270 Ω resistor connected in parallel with the 4–20 mA output converted this to a 1–5 V signal that could be read by one of the 0–5 V analog inputs on a National Instruments (NI) 9381 C series multifunction I/O module. The analog output from the FT2A was recorded using NI LabVIEW$^{\text{TM}}$ interface at a rate of 10 S/s. Measurement accuracy was verified to be within 0.5% during calibration.

An activity temperature controlled sample line was connected to the engine exhaust of generator systems under test and samples were taken continuously during steady state and stochastic load testing. Total hydrocarbons (THC) were measured using a flame ionization detector (Siemens FIDAMAT 6); oxides of nitrogen (NO_x) were measured using a chemiluminescence detector (Siemens NOXMAT 600); carbon monoxide (CO) and carbon dioxide (CO_2) were measured using non-dispersive infrared detectors (Siemens ULTRAMAT 6); exhaust oxygen (O_2) content was measured using a paramagnetic detector (Siemens OXYMAT 6). All emissions were recorded in parts per million (PPM), with the exception of O_2 and CO_2 which were recorded in percent.

5.2. Devices Under Test

In this work, a 22 L NG conventional generator system and an 11 L NG-hybrid generator system were evaluated using the microgrid testbed. Each device under test (DUT) was subjected to an identical series of tests, according to the procedure outlined in section 3.

The conventional generator system was manufactured by Moser Energy Systems (MES) and included a 22 L reciprocating NG engine, with SG rated for 350 kW at 480/277 VAC. A photo of the system is shown in Fig. 7a.

The NG-hybrid generator system was also manufactured by MES, in partnership with LexTM3. This system included an 11 L reciprocating NG engine with a 175 kW, 480/277 VAC SG. The ESM on the unit

[1] 1.00 ft^3/min $= 4.72 \times 10^{-4}$ m^3/s

(a) Conventional 22 L NG genset.

(b) NG-hybrid 11 L generator system with ESM trailer (left) and transformer (right).

Figure 7: Microgrid generator systems installed at CSU Powerhouse.

included a 120 kWh Li-ion battery pack, rated for 240 kW continuous charge/discharge and 360 kW for 10 s. The battery was charged/discharged via a 500 kVA, four-quadrant inverter. The inverter included an externally mounted, 500 kVA 480Δ–480Y/277 V isolation and filtering transformer. The ESM also contained an on-board power distribution bus connecting the ESM, NG genset, and external load ("AC bus" in Fig. 2). The unit was housed on two separate trailer mounts; one trailer housed the NG genset while the other housed the ESM. A photo of the complete NG-hybrid generator system system is shown in Fig. 7b.

In the NG-hybrid generator system system, controller area network bus (CANbus) communication between the ESM and genset controllers allowed the ESM to serve as system-level controller to monitor the NG genset and issue start/stop commands. When load was below a specified threshold, the genset received a "remote stop" command, and the load was served by the ESM only. When load exceeded the low load threshold, the generator received a "'remote start" command.

The ESM inverter and genset in the NG-hybrid generator system used a droop control scheme [22, 23] to maintain the genset at full rated load when the ESM and genset subsystems were running in parallel. Whenever the genset was running, the ESM inverter adjusted its output frequency to maintain the genset at full load (175 kW). Excess energy not consumed by the load was used to charge the battery until it reached a complete state-of-charge (SOC), at which point the genset was cycled off again. At high loads, the battery discharged and the load was served by the parallel combination of ESM and genset power.

6. Experimental Results: Thermal Efficiency

This section demonstrates the analyses of thermal efficiency using measurements from the proposed test procedure applied to the two DUTs described in the previous section.

6.1. Estimating Thermal Efficiency

Thermal efficiency, η, is defined herein as the ratio of total energy delivered to the load, E_{out}, by the total energy supplied to the generator system, E_{in}, i.e., $\eta = {}^{E_{out}}/_{E_{in}}$. Energy into the hybrid generator system originated from two sources: the NG fuel and the stored energy in the battery. Instantaneous power into the hybrid generator system, p_{in}, was thus computed as:

$$p_{in} = v_{bat} i_{bat} + \gamma \frac{dm}{dt}, \tag{3}$$

where v_{bat} [V] is the battery voltage, i_{bat} [A] is the battery current, m is mass of the fuel [kg], ${}^{dm}/_{dt}$ is the mass flow rate of the fuel input [m^3/s], and γ is a conversion factor from [m^3/s] to watts [J/s]. Since the voltage and current supplied by the battery generally changed during testing (e.g., based on the battery SOC) the input energy was computed by integrating the instantaneous power (3) with respect to time, yielding:

$$E_{in} = \int_{t_0}^{t_0+t_d} v_{bat}(\tau) i_{bat}(\tau)\, d\tau + \gamma\, \left(m(t_0+t_d) - m(t_0)\right), \tag{4}$$

where t_0 is the initial starting time of the test, t_d is the test duration, and τ is a dummy integration variable. In the conventional generator system, the input energy was computed from (3)-(4) with $v_{bat} = i_{bat} = 0$.

The generator system output voltages and currents delivered to the load were steady AC waveforms during the testing period; thus steady-state AC circuit analysis was applied to compute average output power. Average power delivered by the generator system, P_{out}, was calculated as the sum of the average power delivered to the load, P_{load}, less average cable power losses, P_{loss}, as:

$$\begin{aligned} P_{out} &= P_{load} + P_{loss} \\ &= 3VI\cos(\theta) + 3I^2 \left(\frac{V_{NL} - V_{FL}}{I_{FL}}\right), \end{aligned} \tag{5}$$

where V, I, and θ are the voltage, current and power factor angle at the load, respectively; V_{NL}, V_{FL}, and I_{FL} are the voltage at the load under no-load conditions, voltage and current at the load under full-load conditions, respectively; all voltages and currents in (5) are expressed as rms. Total output energy during the test was therefore $E_{out} = P_{out} t_d$.

6.2. Thermal Efficiency: Constant Load Tests

During constant load testing, four loads were supplied by the generator systems: 50 kW, 100 kW, 200 kW, and 350 kW. Each load was held constant for $t_d = 20$ min, and the first and last 60 s of each step were discarded to remove transients. Each constant load measurement was repeated three times. Total thermal efficiencies were then calculated and averaged over the three trials for each load.

Table 1 summarizes the thermal efficiency estimates and fuel use during the constant load tests for the conventional and hybrid units. Additionally, for the hybrid unit, the fuel savings when compared against the conventional generator is given. Note that for the first load step, 50 kW, the hybrid unit was operating on battery only. Therefore, no fuel was used for this step, and fuel savings were effectively 100%. However, note that if the load was held indefinitely the generator would be called to recharge the battery, necessitating fuel usage.

Table 1: Constant Load Thermal Efficiency & Fuel Use.

	Conventional		Hybrid		
Load [kW]	**Fuel Used** [m^3]	η [%]	**Fuel Used** [m^3]	η [%]	**Fuel Saved** [%]
50	9.1	15.6	0	86.5	$+100^{\dagger}$
100	13.0	22.4	13.9	23.3	-7.0
200	20.9	29.0	14.0	35.9	$+28.5$
350	30.4	31.6	15.0	48.4	$+50.1$

† With ESM in "battery only" mode.

6.3. Thermal Efficiency: Stochastic Load Tests

During stochastic load testing, a load profile based on the synthesized points in Fig. 5 was programmed on the load bank, as shown in Fig. 8. Each of the 60 samples was held by the load bank for one minute, for a total test duration of $t_d = 3,600\,\text{s}$. The stochastic load sequence was supplied by each generator system over three trials. Total thermal efficiency and fuel usage were calculated and averaged over the the three trials. Measured power delivered to the load during one of the stochastic load tests is shown in Fig. 8.

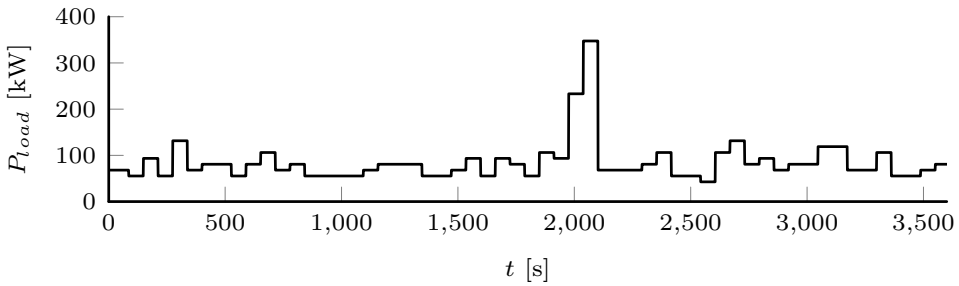

Figure 8: Power supplied to load bank during stochastic load test.

A comparison of fuel flows to the engines in the conventional and hybrid systems is shown in Fig. 9. Note that for the hybrid system, the entire fuel flow curve is shifted downward. Also note that during the peak load, at approximately $t = 2,000\,\text{s}$, the rate of fuel consumption by the conventional generator showed a pronounced surge; in the hybrid system, this peak was met using battery power and generator fuel usage remained relatively flat.

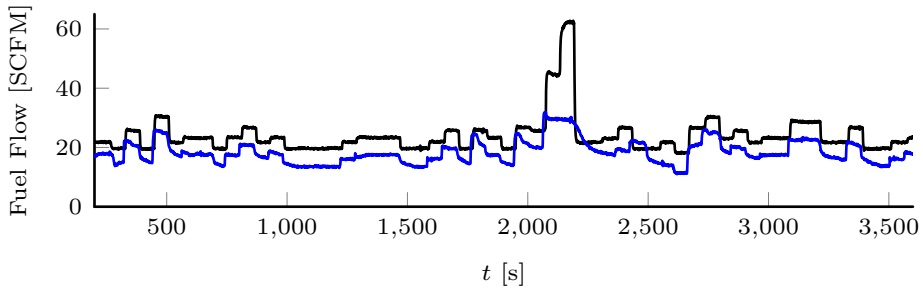

Figure 9: Measured fuel flows for the conventional (black) and hybrid (blue) generator systems during stochastic load tests.

Summarized thermal efficiency and fuel usage for the stochastic load trials are presented in Table 2.

Table 2: Stochastic Load Thermal Efficiency & Fuel Use.

	Conventional		**Hybrid**		
Trial #	**Fuel Used** [m^3]	η [%]	**Fuel Used** [m^3]	η [%]	**Fuel Saved** [%]
1	38.8	20.9	32.7	25.7	+15.9
2	40.6	20.6	31.8	26.1	+21.6
3	40.2	20.3	31.1	26.7	+25.0
Avg.	40.3	20.6	31.9	26.2	+21.0

Discussion: As shown in the preceding experimental results and analysis, the proposed test procedure can be used to draw several conclusions regarding thermal efficiency and fuel usage when comparing conventional and hybrid generator systems. Thermal efficiency for the conventional system was found to range between 15.6% at low load to 31.6% at full load, which indicates reduced efficiency of conventional generator systems under low load conditions. In contrast, thermal efficiency for the hybrid system was found to range between 23.3–86.5%. The lowest thermal efficiency was observed when the generator was simultaneously serving the load and charging the battery; in this mode losses were attributable to the isolation transformer and cabling losses.

Under constant loads, the hybrid system was observed to generally require less fuel than the conventional system. The exception was during 100 kW load testing, when fuel consumption was 7% higher in the hybrid system; this exception is attributable to the hybrid system simultaneously supporting the load while also charging the battery. During stochastic loads, the hybrid generator was observed to have an average 21% fuel savings compared to the conventional system.

The above observations and conclusions indicate the potential usefulness of the test procedure in evaluating types of mobile generator systems, in addition to informing system design and operation. In particular, the above results indicate that proper sizing of the hybrid system based on expected load is critical to ensure fuel savings over conventional systems.

7. Experimental Results: Power Quality

This section demonstrates the assessment of several power quality metrics using the proposed test procedure, applied to the two experimental DUTs.

7.1. Power Quality: Step-load Response

During step-load testing a set of load steps were applied to the generator systems and their output frequency and bus voltages were measured. Transient deviations in the frequency and voltage immediately after the load change, in addition to the "recovery time" to restore nominal frequency and voltage were recorded. Herein, frequency and voltage restoration was defined as being within 1% of pre-disturbance values for at least 10 consecutive electrical cycles.

Step response was measured and evaluated at four load steps: 50 kW, 100 kW, 200 kW, and 350 kW. For each step, the system was initially at no load (0 kW); the load was applied instantaneously and held for one minute, then removed instantaneously. The responses for both load acceptance and load rejection were captured and analyzed.

The absolute value of the frequency deviation, $|\Delta f|$, and recovery time, Δt, for the conventional and hybrid systems is compared in Table 3. Absolute voltage deviations, $|\Delta v|$, and recovery time for both systems is presented in Table 4. Frequency and voltage deviation were calculated as the difference between instantaneous and pre-disturbance values.

Table 3: Frequency deviation and recovery time under step load conditions: Conventional vs. Hybrid.

	Conventional		**Hybrid**	
Load Step [kW]	$\|\boldsymbol{\Delta} f\|$ [Hz]	$\boldsymbol{\Delta} t$ [s]	$\|\boldsymbol{\Delta} f\|$ [Hz]	$\boldsymbol{\Delta} t$ [s]
0–50	1.02	0.56	0.62	0.00
50–0	0.91	0.40	0.54	0.00
0–100	1.93	1.05	1.17	0.02
100–0	1.77	0.89	1.25	0.00
0–200	4.13	3.16	1.25	0.02
200–0	3.65	1.31	1.33	0.00
0–350	36.9	6.47	1.45	0.02
350–0	7.27	1.71	1.36	0.15

Table 4: Voltage deviation and recovery time under step load conditions: Conventional vs. Hybrid.

	Conventional		**Hybrid**	
Load Step [kW]	$\|\boldsymbol{\Delta} v\|$ [pu]	$\boldsymbol{\Delta} t$ [s]	$\|\boldsymbol{\Delta} v\|$ [pu]	$\boldsymbol{\Delta} t$ [s]
0–50	0.014	0.17	0.014	0.09
50–0	0.012	0.15	0.013	0.03
0–100	0.025	0.24	0.031	0.13
100–0	0.026	0.23	0.026	0.11
0–200	0.072	1.64	0.063	2.34
200–0	0.063	0.33	0.058	0.15
0–350	0.566	10.24	0.108	1.07
350–0	0.135	0.53	0.093	0.26

The voltage and frequency response to the largest load acceptance, the 0–350 kW step load, is plotted in Fig. 10. In Fig. 10, v^b_{AB} denotes the bus voltage between phases A and B. As shown in the figure, frequency and voltage deviations in the conventional generator showed a significant overshoot and much longer recovery period in comparison the hybrid system. (Note in this test condition, the internal under-voltage and under-frequency protections on the conventional generator system were disabled to avoid tripping the system offline.)

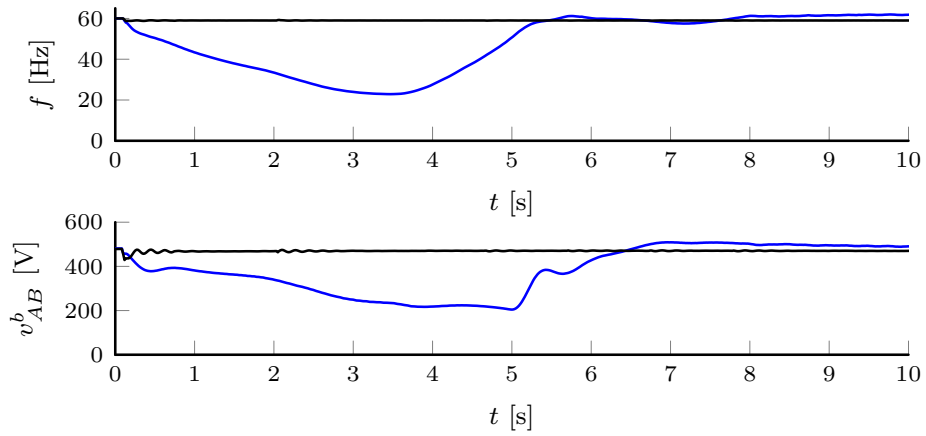

Figure 10: Frequency (top) and voltage (bottom) responses to 0–350 kW step load, conventional (blue) vs. hybrid (black).

7.2. Power Quality: Harmonic Distortion

Total harmonic distortion (THD) of the voltage and current waveforms were evaluated after each load step described above, after transients had settled. Voltage and current waveforms measured at the transfer switch serving the load were recorded at 15.36 kS/s. Fig. 11 shows the voltage and current measurements during a 0–200 kW load step of the conventional generator system. Calculated THD for the bus voltage and current, THD_v and THD_i respectively, during the four load steps and zero load condition shown in Table 5.

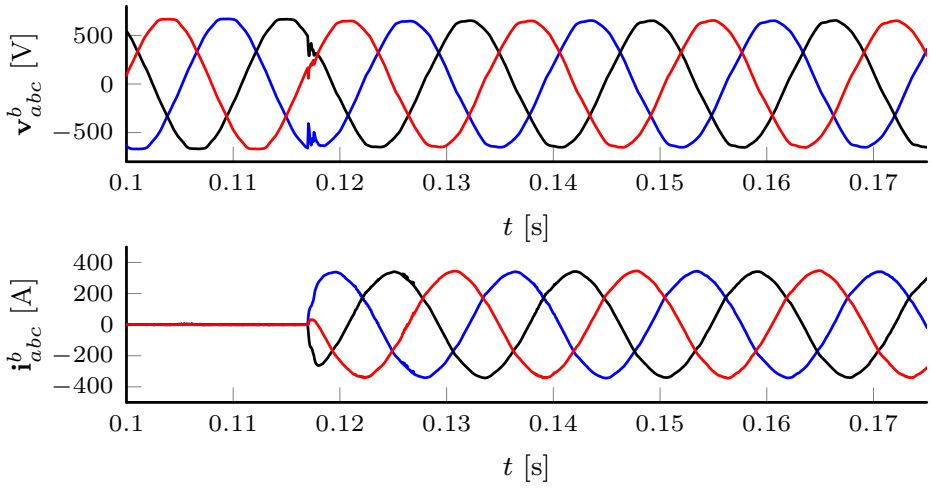

Figure 11: Voltage (top) and current (bottom) from conventional generator during 0–200 kW step load change.

To isolate the harmonic distortion from the ESM, measurement of voltage and current on the delta side of the Δ-Y isolation transformer were also measured; these measurements are shown in Fig. 12.

The waveforms in Fig. 12 were found to contain voltage and current THDs of 1.9% and 19.6%, respectively, due. Individual harmonics in the current due to power-electronic switching in the ESM, determined by a fast Fourier transform (FFT), are plotted in Fig. 13.

In Fig. 13, $||\mathfrak{I}_c(f)||$ denotes the magnitude of the current harmonic at frequency f. As shown in Fig. 13, the current waveform contained discernible harmonic content below 3.5 kHz. Since these harmonics were not observed in the bus current, it can be inferred that they were isolated by the Δ-Y transformer.

Table 5: Total Harmonic Distortion: Conventional vs. Hybrid

	Conventional		**Hybrid**	
Load Step [kW]	$\mathbf{THD}_v$ [%]	$\mathbf{THD}_i$ [%]	$\mathbf{THD}_v$ [%]	$\mathbf{THD}_i$ [%]
0	1.23	–	2.06	–
50	1.75	3.11	2.55	4.38
100	1.81	1.62	1.37	2.50
200	2.64	2.42	1.37	1.49
350	3.36	3.50	1.39	1.34

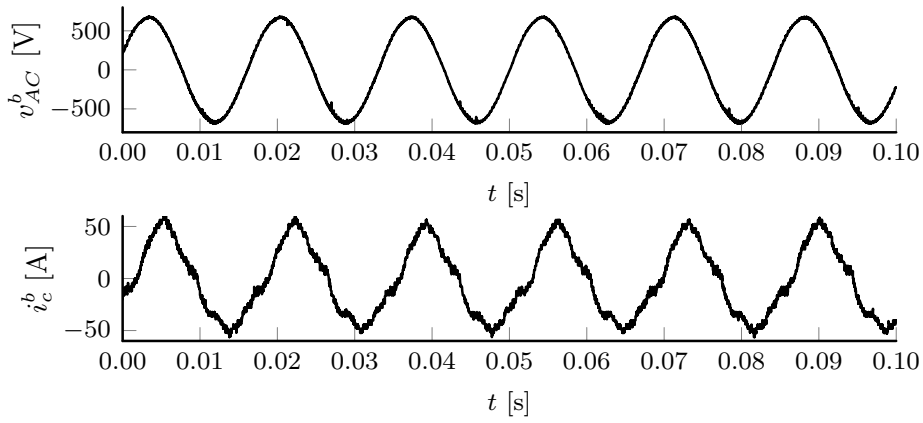

Figure 12: Voltage (top) and current (bottom) on delta side of Δ-Y transformer, hybrid unit under constant 200 kW load.

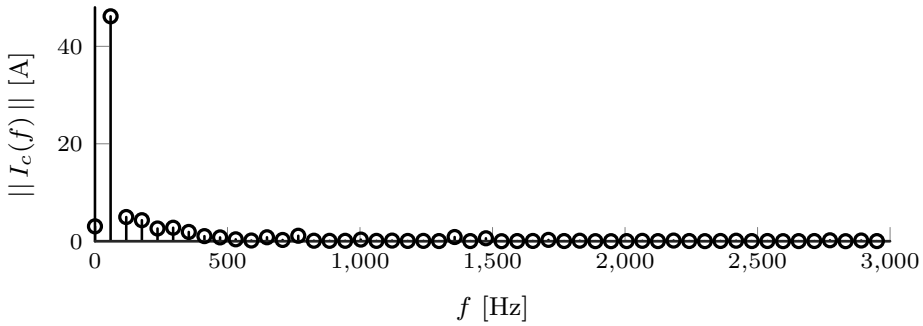

Figure 13: Harmonic spectrum of current i^b_c in Fig. 12.

Discussion: As illustrated above, the test procedure was used to compare various power quality metrics between generator systems. In the experiments shown herein, it was quantitatively demonstrated that the conventional generator system had relatively poor step load performance compared to the hybrid system. General observations based on the results shown in Tables 3 and 4 indicate that frequency response in the conventional generator is poor compared to the hybrid even for small load steps. On the other hand, deviations in voltage response were not that significant between the two systems except during large load steps (in which case, the hybrid system again outperforms in power quality). Voltage and frequency response in both generator systems are controlled by different feedback control mechanisms: for voltage response, feedback is implemented via the exciter, while frequency response is implemented in the governor. Generally, the generator voltage response is fast because the "plant" in the exciter control is an electrical circuit with fast pole dynamics [13]. However, the governor is a slower control response because it includes mechanical components with inertia and the inherent latency of the fuel compressor (not shown in Fig. 1). These differences are the likely explanation for the results in Tables 3 and 4. These observed differences in transient response highlight the potential usefulness of the test procedure for ensuring that particular microgrid load profiles can be served by a generator system without tripping under-voltage and/or under-frequency protection limits specified, e.g., in IEEE 1547-2018 [24].

It was also determined that harmonic distortion at the load was comparable for both generator systems, thus demonstrating the effectiveness of the isolation transformer on the hybrid system to filter current harmonics from power-electronic switching.

As demonstrated above, the proposed test procedure can be used to evaluate competing microgrid generating systems for voltage and frequency stability under a variety of load conditions. This evaluation can aid microgrid system designers in selection and sizing of generator systems based on the expected microgrid load profile. In addition, the procedure can be used to inform the design of isolation or filtering transformers, e.g., to ensure that harmonic content arising from power electronics in hybrid systems is adequately filtered so that power quality at the load is at least comparable to conventional systems.

8. Experimental Results: Emissions

This section demonstrates the analyses of intake NG fuel composition and generator system gas emissions using the experimental generator systems. The chemical analyses in section 8.1 follows the work in [18].

8.1. Estimating Fuel Composition and Exhaust

Before determining exhaust gas emissions, it is necessary to determine the composition of the intake fuel. In this experiment, gas composition analyses were first conducted on the input pipeline natural gas on four separate days just prior to and during testing; gas samples were drawn on 23 Jan, 15 Feb, 12 Mar and 15 Mar of 2019. The gas analyses yielded the molar fractions of hydrocarbon species methane (CH_4) through hexane (C_6H_{14}). For the purposes of these analyses, i-butane (iC_4H_{10}) and n-butane (nC_4H_{10}) were combined, as were i-pentane (iC_5H_{12}) and n-pentane (nC_5H_{12}). The molar fractions of nitrogen (N_2) and carbon dioxide (CO_2), and overall fuel density (ρ) in kilograms per cubic meter [kg/m^3] were also obtained from the analyses. The total molar fraction of the mixture, denoted X, was calculated as the sum of all constituent gases:

$$X = \mathrm{CH_4} + \mathrm{C_2H_6} + \mathrm{C_3H_8} + \mathrm{C_4H_{10}} + \mathrm{C_5H_{12}} + \mathrm{C_6H_{14}} + \mathrm{CO_2} + \mathrm{N_2} \tag{6}$$

Let $\mathcal{L} = \{\mathrm{CH_4}, \ldots, \mathrm{N_2}\}$ denote a set containing the names (labels) of all the gases in (6) and $\mathcal{I}$ be an index set of $\mathcal{L}$. Further, let $\ell_i \in \mathcal{L}$, $i \in \mathcal{I}$ be the i'th label in $\mathcal{L}$.

Because trace organics and other inert gases were not captured, X was slightly less than 100%. The raw molar fractions from a gas composition analysis were therefore first normalized according to:

$$x^*_{\ell_i} = \left(\frac{x_{\ell i}}{X}\right), \tag{7}$$

where $x_{\ell i}$ is the raw molar fraction of gas ℓ_i from a gas composition analysis and $x^*_{\ell i}$ its normalized molar fraction.

The molar mass of each gas $M_{\ell i}$ was then determined by multiplying the normalized molar fraction by the standard atomic weight of each gas. Defining $A_r(\ell_i)$ as a standard atomic weight look-up function for gas ℓ_i, $M_{\ell_i} = A_r(\ell_i)x^*_{\ell i}$ [g/mol]. The total molar mass of the fuel was then computed as the sum of the mass of each constituent gas:

$$M = \sum_i M_{\ell i}, \quad \forall i \in \mathcal{I} \tag{8}$$

The mass fraction $y_{\ell i}$ of each constituent gas was then calculated as $y_{\ell i} = {}^{M_{\ell i}}/_{M}$. The total carbon content of the fuel, based on the chemical formula in (6), was calculated using the normalized molar fractions as:

$$\alpha_C = x^*_{\mathrm{CO_2}} + \sum_{i=1}^{6} i x^*_{\ell i}, \tag{9}$$

and hydrogen content of the fuel was calculated as:

$$\beta_H = \sum_{i=1}^{6} (2+2i) x^*_{\ell i}. \tag{10}$$

It was assumed that the only source of oxygen in the fuel was from CO_2; therefore total oxygen content of the fuel was computed as $\gamma_O = 2x^*_{\mathrm{CO_2}}$. Finally, it was also assumed that the only source of nitrogen in the fuel was the N_2; thus total nitrogen content of the fuel was computed as $\delta_N = 2x^*_{\mathrm{N_2}}$.

The stoichiometric air-fuel ratio, AFR_s, was calculated as:

$$AFR_s = \frac{A_s\left(M_{\mathrm{O_2}} + 3.7742 M_{\mathrm{N_2}}\right)}{A_r(\mathrm{C}) + \frac{\beta_H}{\alpha_C} A_r(\mathrm{H}) + \frac{\gamma_O}{\alpha_C} A_r(\mathrm{O}) + \frac{\delta_N}{\alpha_C} A_r(\mathrm{N})}, \tag{11}$$

where $M_{\mathrm{O_2}}$ and $M_{\mathrm{N_2}}$ are the molar masses of O_2 and N_2, respectively, and A_s is the air portion of AFR_s expressed as:

$$A_s = 1 + \frac{\beta_H}{4\alpha_C} - \frac{\gamma_O}{2\alpha_C}. \tag{12}$$

The exhaust hydrogen fraction, $\mathrm{H_2^{ex}}$, was calculated as

$$\mathrm{H_2^{ex}} = \frac{\frac{\beta_H}{2\alpha_C}\mathrm{CO}^{ex}\left(\mathrm{CO_2^{ex}} + \mathrm{CO}^{ex}\right)}{3.5\,\mathrm{CO_2^{ex}} + \mathrm{CO}^{ex}} \tag{13}$$

where superscript "ex" denotes exhaust gas. By substituting the previously determined molar fractions of C, H, O, and $\mathrm{H_2^{ex}}$ into (11)-(12), the air portion, A, of the actual air-fuel ratio is calculated as:

$$A = \frac{\mathrm{CO_2^{ex}} - \sigma\mathrm{THC}^{ex} + \frac{\mathrm{CO}^{ex}}{2} + \frac{\mathrm{NO_x^{ex}}}{2} + \mathrm{CO}^{ex} - \frac{\mathrm{H_2^{ex}}}{2}}{\mathrm{CO_2^{ex}} + \mathrm{CO}^{ex} + \mathrm{THC}^{ex}} + \sigma,$$

where $\sigma := {}^{\beta_H}/_{4\alpha_C} - {}^{\gamma_O}/_{2\alpha_C}$. Note that all CO^{ex}, THC^{ex} and NO_x^{ex} terms in (13)-(14) must be normalized by a factor of 10^4 since they are measured in ppm; CO_2^{ex} and O_2^{ex} were measured in percent.

The actual air-fuel ratio, AFR, was then calculated as $AFR = ({}^{A}/_{A_s})AFR_s$. The combustion factor, C_f, was calculated as:

$$C_f = \frac{M^{ex}/M^a}{1 + 1/AFR}, \tag{14}$$

where M^{ex} and M^a are the molar masses of the exhaust and air, respectively. M^a is a known constant with a value of 28.97 [g/mol]; since M^{ex} was unknown, the ratio ${}^{M^{ex}}/_{M^a}$ was assumed to be 0.98.

The brake specific emissions coefficient, B, was computed as:

$$B = \frac{{}^{dm}/_{dt}}{\mu P_e \left(\text{THC}^{ex} + \text{CO}^{ex} + 0.01\text{CO}_2^{ex} + C_f\text{CO}_2^a\right)}, \tag{15}$$

where ${}^{dm}/_{dt}$ is mass flow rate [kg/m^3], P_e [kW] is the electric power delivered to the load, CO_2^a (= 409 ppm) is the atmospheric concentration of CO_2 in the air, and

$$\mu := A_r(\text{C}) + \frac{\beta_H}{\alpha_C}A_r(\text{H}) + \frac{\gamma_O}{\alpha_C}A_r(\text{O}) + \frac{\delta_N}{\alpha_C}A_r(\text{N}). \tag{16}$$

Brake specific emissions, $B_{\ell i}$ [g/kWh], for a particular gas $\ell i \in \mathcal{L}$ was calculated using (7)-(8) and (15) as:

$$B_{\ell i} = BM_{\ell i}\, x^*_{\ell i}, \quad \forall i \in \mathcal{I}. \tag{17}$$

8.2. Emissions Analysis: Constant Load

During constant load emissions testing, gas emissions were calculated using the brake specific emission calculation described above, evaluated at the same constant loads described in section 6.2. As in the thermal efficiency measurements, data was collected over three trials and the first and last 60 s of each measurement were discarded to eliminate transients. A comparison of the emissions between the conventional and hybrid systems is given in Table 6.

8.3. Emissions Analysis: Stochastic Load

Emissions were also evaluated for the conventional and hybrid systems under the stochastic load profile described in section 6.3. Emissions for the four pollutants, averaged across the three trails, were measured. A comparison of the emissions in the conventional and hybrid systems is given in Table 7.

Discussion: As described above, the test procedure was used to compare emissions between generator systems. When comparing the exhaust emissions under constant load in the experimental systems, it was observed that THC, CO, and CO_2 were lower at three points (50 kW, 200 kW, and 350 kW) in both types. However, at 100 kW, emissions were elevated in the hybrid system relative to the conventional system, likely because at this load the hybrid NG genset was also charging the battery (see section 6.2, Table 1). NO_x emissions were observed to be elevated at the middle load points; further investigation indicated that this was likely the result of oxygen saturation in the engine catalyst under the specific engine control settings during testing (cf. [25]).

Emission of greenhouse gases while supplying stochastic loads, specifically THC and CO_2, were found to be reduced significantly in the hybrid system, while emissions of CO and NO_x were found to increase; the later observation is suspected to be a result of oxygen saturation on the catalyst.

As illustrated in the above analysis, the proposed test procedure can be used to evaluate competing microgrid generating systems in terms of gas emissions. As indicated above, this analysis can also inform system design modifications, e.g., tuning engine fuel controls for minimizing gas emissions under expected microgrid load conditions.

Table 6: Constant Load Emissions: Conventional vs. Hybrid.

Gas	**Load** [kW]	**Conv.** [g/kWh]	**Hybrid** [g/kWh]	**Δ** [%]
THC	50	0.70	0.00	$-100.0^{\dagger\dagger}$
	100	0.31	0.87	$+180.6$
	200	0.91	0.52	-43.4
	350	0.94	0.29	-68.8
CO	50	0.56	0.00	-100.0
	100	0.65	1.05	$+61.5$
	200	0.91	0.85	-6.6
	350	1.37	0.52	-62.0
NO_x	50	0.67	0.00	-100.0
	100	0.17	0.68	$+306.0$
	200	0.11	0.32	$+191.0$
	350	0.18	0.20	-7.3
CO_2	50	1,325.60	0.00	-100.0
	100	923.37	1001.33	$+8.4$
	200	715.47	537.77	-24.8
	350	659.13	309.70	-53.0

†† With ESM in "battery only" mode.

Table 7: Stochastic Load Emissions: Conventional vs. Hybrid.

Gas	**Conv.** [g/kWh]	**Hybrid** [g/kWh]	**Δ** [%]
THC	0.78	0.43	-44.7
CO	0.79	0.89	$+12.2$
NO_x	0.24	0.54	$+123.6$
CO_2	1072.9	892.2	-16.8

9. Case Study: Economic and Environmental Analysis

This section presents an economic and environmental analysis to demonstrate how the measurements obtained from the test procedure described in the foregoing can be used to compare conventional versus hybrid generator configurations in an example design case study.

In this study, the following assumptions are made. A microgrid generating system is being designed to serve an off-grid electrical load; the 22 L conventional and 11 L hybrid generating systems described in section 5.2 are the alternative systems under consideration. For simplicity it is assumed that the load consists of constant powers contained in the vector $\mathbf{P} = [\,50\ 100\ 200\ 350\,]^T$ kW. For a majority of the time (96%), the load demand varies evenly between the power levels 50, 100, and 200 kW, and for the remaining 4% of the time, the load is 350 kW. This situation corresponds to an off-grid system with moderate nominal load

demand with infrequent, but large, power demands (conditions that may be observed in mining and drilling applications). Let $\mathbf{w} = [0.32\ 0.32\ 0.32\ 0.04]^T$ denote a weighting vector associated with the amount of time the load is at a given power level. Then the average power is computed as:

$$P_{avg} = \mathbf{w}^T\mathbf{P} = \sum_i w_i P_i = 126\,\text{kW} \tag{18}$$

From Table 6, vectors for emissions are defined as $\mathbf{THC}_c = [0.70\ 0.31\ 0.91\ 0.94]^T$, $\mathbf{THC}_h = [0.00\ 0.87\ 0.52\ 0.29]^T$, $\mathbf{CO}_c = [0.56\ 0.65\ 0.91\ 1.37]^T$, $\mathbf{CO}_h = [0.00\ 1.05\ 0.85\ 0.52]^T$, $\mathbf{NO}_{x,c} = [0.67\ 0.17\ 0.11\ 0.18]^T$, $\mathbf{NO}_{x,h} = [0.00\ 0.68\ 0.32\ 0.20]^T$, $\mathbf{CO}_{2,c} = [1325.6\ 923.4\ 715.5\ 659.1]^T$, $\mathbf{CO}_{2,h} = [0.00\ 1001.3\ 537.8\ 309.7]^T$, where all units are in g/kWh, the subscript "c" denotes conventional and "h" denotes hybrid. Total emissions for the four gases measured in the test procedure which are produced by the conventional system in g/kWh is estimated as:

$$E_c = \mathbf{w}^T\left(\mathbf{THC}_c + \mathbf{CO}_c + \mathbf{NO}_{x,c} + \mathbf{CO}_{2,c}\right). \tag{19}$$

Let $T = 8,760$ hr be the total operational time of the system per year. Then the total emissions generated by the conventional system is $E_c P_{avg} T/1000 = 1.08 \times 10^6$ kg. A similar calculation for the hybrid system yields total emissions of 0.55×10^6 kg, representing a 48% reduction in total emissions in the hybrid system.

For estimating fuel costs, from Table 1, vectors of fuel rates[1] are defined as $\mathbf{F}_c = [27.3\ 39.0\ 62.7\ 91.2]^T$, $\mathbf{F}_h = [0.0\ 41.7\ 44.7\ 45.0]^T$ in units of m^3/hr. Fuel cost, f_c, for the conventional generator is computed:

$$f_c = C_{ng} T\left(\mathbf{w}^T\mathbf{F}_c\right), \tag{20}$$

where C_{ng} is the cost of NG fuel. Using the average monthly fuel cost for NG from 2001 to 2021 [21], $C_{ng} = 0.19$ [\$USD/m^3], total yearly fuel costs for the conventional generator are estimated at \$75.9k; a similar calculation for the hybrid generator yields fuel costs per year of \$49.8k, representing a fuel usage reduction of 34% for the hybrid system relative to the conventional.

In this study, the purchase cost for the conventional system is assumed to be \$140k. The purchase cost for the hybrid system, \$260k, is assumed to be greater than the conventional generator; although the engine size is smaller, the ESM adds additional capital equipment costs. Maintenance costs between the conventional and hybrid systems are significantly different based on the environmental monitoring rules. In the US for example, engines with over a 500 hp nameplate rating require monthly emissions readings [9]. In the 22 L NG engine described in section 5.2, engine horsepower is 507 hp. Required emissions readings for the conventional system require an estimated \$10k in monitoring equipment and monthly service costs of \$1.5k, which includes basic monthly maintenance costs of \$0.1k plus \$1.4k in service and administration fees associated with the emissions readings. In contrast, the hybrid system contains an 11 L NG 268 hp engine. The hybrid system therefore does not require the additional emissions monitoring equipment or readings and has a monthly service cost of \$0.1k to cover basic maintenance.

A summary comparison of the economic and environmental costs associated with the alternative generating systems are shown in Table 8.

[1] Note that the values in Table 1 were obtained over 20 min testing intervals; these values have been scaled by a factor of 60⁄20 to obtain hourly fuel consumption rates.

Table 8: Summary of Economic and Environmental Costs: Conventional vs. Hybrid.

Description	**Conventional**	**Hybrid**
Purchase Costs† [$] $\times 10^3$	140	260
Additional Equipment costs [$] $\times 10^3$	10	–
Monthly Service Costs [$] $\times 10^3$	1.5	0.1
Monthly Fuel Costs [$] $\times 10^3$	6.3	4.1
Total Emissions [kg] $\times 10^6$	1.1	0.6

† For illustration purposes only; not an official price quote.

As shown in Table 8, the difference in upfront economic costs (including initial purchase and additional equipment) for the conventional system is $\$150$k lower than the hybrid system. However, thereafter, monthly maintenance and operating (M&O) costs (including monthly service and fuel costs) for the conventional system are $\$3.6$k higher than in the hybrid system. Neglecting changes in M&O costs and the time value of money, the additional upfront costs of the hybrid system would amortize in approximately 30 months (2.5 yrs), and the hybrid system would generate 48% less emissions during its service life relative the conventional system.

Other factors in considering the alternative systems are enhanced power quality and short-term backup power redundancy of the hybrid system. Although not analyzed in detail here, enhanced power quality despite large peak load demands obtained in the hybrid system could result in better local equipment reliability. In addition, the battery in the hybrid ESM can provide short-term backup power, e.g., after an emergency loss or interruption in the NG fuel supply. Based on the considerations above, the hybrid system may be the most attractive choice in terms of economic, environmental, and reliability considerations particularly for service lifetimes of over 2.5 yrs.

10. Conclusions

This paper proposed a test procedure for evaluating and comparing mobile microgrid generator systems in terms of several power and environmental metrics. These metrics included (*i*) thermal efficiency, under constant and stochastic loads, (*ii*) voltage and frequency deviations under load step changes, (*iii*) steady-state voltage and current distortion under constant loads, and (*iv*) engine emissions for four types of atmospheric pollutants, under constant and stochastic loads. The procedure included a load synthesis step for creating stochastic test load profiles based on field measurements. A detailed gas composition and emissions analysis was performed. In addition, this paper described an example microgrid testbed for implementing the procedure which included power hardware and equipment, cabling, sensing and data acquisition, and software control.

The proposed test procedure was experimentally demonstrated on two types of systems with differing engine sizes: a conventional 22 L NG genset and a hybrid system consisting of an 11 L NG genset in parallel with a battery energy storage. IIt was found that the procedure could be used to observe significant differences in power quality, fuel usage and emissions of the gases in the two configurations. These experimental measurements were used to illustrate an economic and environmental cost analysis comparing the two configurations for an off-grid system requiring infrequent but high peak instantaneous power requirements, e.g., for remote mining or drilling applications.

In addition to the metrics stated in the test procedure, the experiments and analysis described in this paper indicated other potential uses of the procedure by generator and microgrid system designers. First,

it was noted that the procedure could be used to size and control hybrid systems to maximize fuel savings, under expected loads, relative to conventional systems. Second, the procedure can be used to determine whether microgrid generator systems will violate protection settings under representative microgrid loads. Third, while evaluating generator systems in terms of gas emissions, the measurements may inform the tuning of fuel controls to minimize their emissions under expected microgrid loads. Forth, experimental measurements using the proposed procedure may be used to tune high-fidelity generator system models to enable detailed generator response and system optimization studies. Finally the test procedure may be useful for obtaining experimental measurements on mobile microgrid generators providing power to land-based gas drilling operations; these measurements could provide inputs to large, system-level economic and environmental trade-off studies for the shale gas supply chain (cf. [26, 27]).

Acknowledged limitations of this work are that only two microgrid system types were evaluated. These systems were also both NG engines of different sizes; potential secondary differences that could arise in the capacity factors (loading) on the engines and their comparative significance were not considered. In addition, other potential power quality metrics such as voltage/current imbalance, voltage fluctuation, and under-voltage were not examined. Further refinement and validation of the test procedure for different engine types, consideration of engine capacity, additional fuel compositions (e.g., diesel fuel) and additional power quality metrics are recommended for future work. Nevertheless, in light of the initial experimental results described in this paper, the authors propose the test procedure for evaluation and comparison of mobile microgrid systems in terms of power quality, emissions, and to inform microgrid design studies.

Acknowledgments

The authors wish to thank Moser Energy Systems for their sponsorship of this work, for providing the test units, operational training and technical support. We thank Spirae for their on-site technical support and use of the InteGrid load bank, and LexTM3 for their technical support on the ESM. We also thank the editorial reviewers of this manuscript for their thorough and thoughtful feedback.

Funding

This work was supported by Moser Energy Systems, Evansville, WY (USA), under a sponsored industry-university research agreement.

References

[1] S. N. Bhaskara and B. H. Chowdhury, "Microgrids—a review of modeling, control, protection, simulation and future potential," *IEEE Power and Energy Society General Meeting*, pp. 1–7, 2012.

[2] Z. Ye, R. Walling, N. Miller, P. Du, and K. Nelson, "Facility Microgrids Facility Microgrids," National Renewable Energy Laboratory, Subcontract Report NREL/SR-560-38019, 2005.

[3] Microgrids at Berkeley Lab, "Types of Microgrids," 2019. [Online]. Available: https://building-microgrid.lbl.gov/types-microgrids

[4] C. Lute, T. L. Conrad, S. A. Kenner, and C. L. Tremel, "Mission critical infrastructure for installations," in *2012 IEEE PES Innovative Smart Grid Technologies (ISGT)*. Washington, DC, USA: IEEE, Jan. 2012, pp. 1–5.

[5] *The New Orleans Hurricane Protection System: What Went Wrong and Why: A Report by the American Society of Civil Engineers Hurricane Katrina External Review Panel*, 2007. [Online]. Available: http://www.asce.org/uploadedFiles/Publications/ASCE{_}News/2009/04{_}April/ERPreport.pdf

[6] L. Che and M. Shahidehpour, "Adaptive Formation of Microgrids With Mobile Emergency Resources for Critical Service Restoration in Extreme Conditions," *IEEE Transactions on Power Systems*, vol. 34, no. 1, pp. 742–753, 2019.

[7] Y. Han, P. M. Young, A. Jain, and D. Zimmerle, "Robust control for microgrid frequency deviation reduction with attached storage system," *IEEE Transactions on Smart Grid*, vol. 6, no. 2, pp. 557–565, 2015.

[8] CIMAC Working Group on Gas Engines, "Transient Response Behaviour of Gas Engines," International Council on Combustion Engines, Tech. Rep., Apr. 2011. [Online]. Available: https://www.cimac.com/cms/upload/Publication_Press/WG_Publications/CIMAC_WG17_2011_Apr_Position_TransResp.pdf
[9] *Protection of the Environment*, U.S. Code of Federal Regulations. Title 40, §60, 2019.
[10] K. Kim, K. Park, J. Lee, K. Chun, and S.-H. Lee, "Analysis of Battery/Generator Hybrid Container Ship for CO_2 Reduction," *IEEE Access*, vol. 6, pp. 14 537–14 543, 2018.
[11] S. J. Ericson and D. R. Olis, "A Comparison of Fuel Choice for Backup Generators," National Renewable Energy Laboratory, Technical Report NREL/TP–6A50-72509, Mar. 2019.
[12] S. P. Makhija and S. P. Dubey, "Analysis of effects on hybrid power system's costs and pollutant emissions due to replacement of petroleum diesel with natural gas, fuel oil and biodiesel," in *2016 3rd International Conference on Electrical Energy Systems (ICEES)*. Chennai, India: IEEE, Mar. 2016, pp. 276–282.
[13] P. Krause, O. Wasynczuk, S. Sudhoff, and S. Pekarek, *Analysis of Electric Machinery and Drive Systems, 3rd Edition*. Hoboken, NJ: Wiley, IEEE Press, 2013.
[14] R. Acosta, "Comparing Natural Gas and Diesel Generator Sets," *Power Engineering*, vol. 119, no. 2, Feb. 2015. [Online]. Available: https://www.power-eng.com/2015/02/13/comparing-natural-gas-and-diesel-generator-sets/#gref
[15] U.S. Environmental Protection Agency, "AP 42, Fifth Edition Compilation of Air Pollutant Emissions Factors, Volume 1: Stationary Point and Area Sources," EPA, Technical Report, 2000.
[16] O. Badr, S. Probert, and P. O'Callaghan, "Atmospheric methane: Its contribution to global warming," *Applied Energy*, vol. 40, no. 4, pp. 273–313, Jan. 1991. [Online]. Available: https://linkinghub.elsevier.com/retrieve/pii/030626199190021O
[17] A. Khaligh and Zhihao Li, "Battery, Ultracapacitor, Fuel Cell, and Hybrid Energy Storage Systems for Electric, Hybrid Electric, Fuel Cell, and Plug-In Hybrid Electric Vehicles: State of the Art," *IEEE Transactions on Vehicular Technology*, vol. 59, no. 6, pp. 2806–2814, Jul. 2010.
[18] C. M. Urban and C. A. Sharp, "Computing Air/Fuel Ratio from Exhaust Composition," *ASME ICE Conference Proceedings on Natural Gas and Alternative Fuels for Engines*, vol. 24, 1994.
[19] L. Devroye, *Non-Uniform Random Variate Generation*. New York, NY: Springer-Verlag, 1986.
[20] Spirae, "InteGrid Test and Development Laboratory," 2018. [Online]. Available: https://www.spirae.com/integrid-lab/
[21] U.S. Energy Information Administration, "United States Natural Gas Industrial Price," 2021. [Online]. Available: https://www.eia.gov/dnav/ng/hist/n3035us3m.htm
[22] M. E. Susetyo, N. Hariyanto, A. Rizqiawan, and S. A. Sitompul, "Droop control implementation on hybrid microgrid PV-diesel-battery," in *2017 International Conference on High Voltage Engineering and Power Systems (ICHVEPS)*. Bali: IEEE, Oct. 2017, pp. 295–300.
[23] X. Lu, J. M. Guerrero, K. Sun, J. C. Vasquez, R. Teodorescu, and L. Huang, "Hierarchical Control of Parallel AC-DC Converter Interfaces for Hybrid Microgrids," *IEEE Transactions on Smart Grid*, vol. 5, no. 2, pp. 683–692, Mar. 2014.
[24] *IEEE Standard for Interconnection and Interoperability of Distributed Energy Resources with Associated Electric Power Systems Interfaces*, IEEE Std. 1547–2018, 2018.
[25] E. P. Brandt, Y. Wang, and J. W. Grizzle, "Dynamic modeling of a three-way catalyst for SI engine exhaust emission control," *IEEE Transactions on Control Systems Technology*, vol. 8, no. 5, pp. 767–776, 2000.
[26] Y. Chen, L. He, Y. Guan, H. Lu, and J. Li, "Life cycle assessment of greenhouse gas emissions and water-energy optimization for shale gas supply chain planning based on multi-level approach: Case study in Barnett, Marcellus, Fayetteville, and Haynesville shales," *Energy Conversion and Management*, vol. 134, pp. 382–398, 2017.
[27] Y. Chen, L. He, J. Li, and S. Zhang, "Multi-criteria design of shale-gas-water supply chains and production systems towards optimal life cycle economics and greenhouse gas emissions under uncertainty," *Computers and Chemical Engineering*, vol. 109, pp. 216–235, 2018.